Biomaterials 31 (2010) 2272–2277

Contents lists available at ScienceDirect

Biomaterials

journal homepage: www.elsevier.com/locate/biomaterials

# Bioconjugation of barium titanate nanocrystals with immunoglobulin G antibody for second harmonic radiation imaging probes

Chia-Lung Hsieh [a,b,*], Rachel Grange [a], Ye Pu [a], Demetri Psaltis [a]

[a] School of Engineering, EPFL, Station 17, 1015 Lausanne, Switzerland
[b] Department of Electrical Engineering, California Institute of Technology, 1200 East California Boulevard, MC 136-93, Pasadena, CA 91125, USA

ARTICLE INFO

*Article history:*
Received 9 November 2009
Accepted 26 November 2009
Available online 8 December 2009

*Keywords:*
Confocal microscopy
Cross-linking
Immunochemistry
In vitro test
Nanoparticle
Surface modification

ABSTRACT

The second harmonic generation (SHG) active nanocrystals have been demonstrated as attractive imaging probes in nonlinear microscopy due to their coherent, non-bleaching and non-blinking signals with a broad flexibility in the choice of excitation wavelength. For the use of these nanocrystals as biomarkers, it is essential to prepare a chemical interface for specific labeling. We developed a specific labeling scheme for barium titanate ($BaTiO_3$) nanocrystals which we use as second harmonic radiation imaging probes. The specificity was achieved by covalently coupling antibodies onto the nanocrystals. We demonstrate highly specific labeling of the nanocrystal conjugates in an antibody microarray and also the membrane proteins of live biological cells in vitro. The development of surface functionalization and bioconjugation of SHG active nanocrystals provides the opportunities of applying them to biological studies.



## 1. Introduction

Detecting and tracing specific molecules of interest are important for studying the function and the behavior of biological systems. Biomarkers have been developed to achieve this goal by creating a contrast between signal and background. An extremely effective method to obtain such contrast is to shift the radiated signal away from the excitation wavelength so that the excitation can be efficiently removed by optical filters. Several mechanisms of converting the wavelength have been demonstrated, such as single-photon and multi-photon fluorescence [1–5], endogenous SHG [6–10], and third harmonic generation (THG) [7,11–13]. Among them, fluorescent biomarkers such as green fluorescent proteins (GFPs) [1], organic dyes [2], and quantum dots (QDs) [4] have been widely used for biomedical imaging due to their excellent brightness and biocompatibility.

We have developed $BaTiO_3$ nanocrystals [14,15] as biomarkers using the SHG signal from nanoparticles [16–30]. We refer to these probes as "Second Harmonic Radiation IMaging Probes (SHRIMPs)". When a nanocrystal of non-centrosymmetric structure is optically excited at a fundamental frequency, it emits the optical signal at the exact doubled frequency. Materials with crystalline structure lacking a center of symmetry are capable of efficient SHG, while centrosymmetric materials have a weak SHG response mostly from the surface where the symmetry is broken [31]. Thus, when imaged at the second harmonic frequency, SHRIMPs provide an effective contrast mechanism between the markers and the generally unstructured or isotropic biological environment. Ordered and highly polarizable biological non-centrosymmetric structures, such as collagen fibers, have endogenous SHG [6–10]. However, in most biological cell components, the endogenous SHG from the cell interface layers is weak [32].

Unlike fluorescence, the SHG process only involves virtual electron energy transition without nonradiative energy loss. Owing to this virtual transition process, SHRIMPs do not bleach over time and emit a stable, non-blinking signal that does not saturate with increasing excitation power. Furthermore, the response time of SHG process is in the femtosecond scale, which is four to five orders of magnitude faster than typical fluorophores. This allows for the observation of fast dynamic processes over a long time. In addition, SHG is generally a non-resonant process which offers broad flexibility in the choice of excitation wavelength. The coherent nature of the SHG signal is also a major advantage, providing a possibility to detect the second harmonic signal generated from the nanocrystals with interferometric optical techniques [14,15,18].

The SHG properties of several kinds of nanocrystals have been recently reported: $BaTiO_3$ [14,15,25], ZnO [16,23,26], $KTiOPO_4$ (KTP) [18,22,24,27], $Fe(IO_3)_3$ [20,30], $KNbO_3$ [21], $Sr_{0.6}Ba_{0.4}Nb_2O_6$ [28], organic nanocrystals [17], and SHG active crystalline

* Corresponding author at: School of Engineering, EPFL, Station 17, 1015 Lausanne, Switzerland.
*E-mail address:* chia-lung.hsieh@epfl.ch (C.-L. Hsieh).

0142-9612/$ – see front matter © 2009 Elsevier Ltd. All rights reserved.
doi:10.1016/j.biomaterials.2009.11.096

organic-inorganic hybrid nanoparticles [19,29]. In our previous work, we have characterized the SHG response from individual $BaTiO_3$ nanocrystals and also used them as SHRIMPs for non-specific cell labeling [15]. For most biological applications, it is essential to prepare a chemical interface for specific labeling. The surface functionalization of these SHG active dielectric nanomaterials can be limited by lack of compatibility between the inorganic nanoparticles and the organic bio-molecules. It has been reported that SHG and sum-frequency-generation active ZnO nanocrystals can be stabilized in aqueous suspension and further incorporated with the folic acid molecules for tumor cell targeting when being encapsulated in phospholipid micelles [23]. In this paper, we demonstrate the specific labeling of $BaTiO_3$ nanocrystals by directly conjugating immunoglobulin G (IgG) antibody on the surface of the nanocrystals. To the best of our knowledge, this is the first demonstration of functionalized SHG nanocrystals by covalently coupling the antibody to the surface of the nanocrystals. The antibody conjugation provides a flexible scheme to target a specific molecule in a biological specimen.

## 2. Experimental section

### 2.1. Materials

$BaTiO_3$ nanocrystals in dry powder were commercially available from Tech-Powder (TechPowder S.A. Lausanne, Switzerland). Nitric acid (65%) and ammonia (25%) were purchased from AnalaR Normapur, VWR. 3-aminopropyltriethoxysilane (APTES, >98%), ethylenediaminetetraacetic acid (EDTA, >99.99%), 2-mercaptoethanol (>98%), DL-dithiothreitol (DTT, 1M), bovine serum albumin (BSA, >98%), Tween 20, and Gelatin were purchased from Sigma–Aldrich. Ethanol (>99.8%) was obtained from Fluka. Sulfosuccinimidyl 4-[*N*-maleimidomethyl]cyclohexane-1-carboxylate (sulfo-SMCC) was obtained from Thermo Scientific. 2-(N-morpholino)ethanesulfonic acid (MES, 0.5 M) was purchased from Biochemika Ultra. The exchange buffer was composed of 50 mM of MES and 2 mM of EDTA in distilled water pH 7. Phosphate-buffered salines (PBS pH 7.4), Dulbecco's Modified Eagle Medium with high glucose (DMEM), fetal bovine serum (FBS), and Calcein AM (C3100MP) were obtained from Invitrogen. Four types of primary antibodies used in this work were Mouse anti-Human IgG (CD144, VE-caderin, BD Biosciences), Goat anti-Human IgG (Jackson ImmunoResearch), Rabbit anti-Human IgG (Jackson ImmunoResearch), and Mouse monoclonal antibody specific to human HLA class I antigens (MHBC01, Invitrogen). The secondary antibody was a Donkey anti-Mouse IgG antibody-Cy5 (Jackson ImmunoResearch).

### 2.2. Antibody microarray preparation

Three different types of the primary antibodies and also the buffer solution were printed separately and repeatedly on the slide in the form of a microarray. The three types of the primary antibodies were Mouse anti-Human IgG (CD144), Goat anti-Human IgG, and Rabbit anti-Human IgG. The Mouse anti-Human IgG was the target primary antibody because the secondary antibody was an anti-Mouse IgG. The primary antibodies were printed on the aldehydesilane coated slides (Nexterion Slide AL, Schott Nexterion) by a contact-printing robotic microarrayer (OmniGrid 300, Genomic Solutions) equipped with SMP2 pins (TeleChem International) at 22 °C with 60% relative humidity. The spotting buffer solution was PBS with 5% glycerol, and the concentration of the primary antibody was 0.2 mg/mL. The size of the printing spot is 90 μm in diameter and the period between two adjacent spots is 200 μm. After printed, the slides were incubated for an hour at 22 °C at 75% relative humidity. During the incubation, the proteins cross-linked to the slide. Then the free aldehyde groups on the slides were blocked by 50 mM triethanolamine (titrated to pH 8 with boric acid) for 30 min at room temperature. The slide was rinsed by water and then dried by centrifugation.

### 2.3. HeLa cell culture and immunostaining

HeLa cell line was provided by the Biomolecular Screening Facility at EPFL, Switzerland. The HeLa cells were grown in flasks containing the growth media (DMEM supplemented with 10% heat-inactivated FBS) at 37 °C in a humidified atmosphere of 5% $CO_2$. The HeLa cells were harvested from the flask by applying Trypsin for 4 min at 37 °C. We counted and prepared $10^6$ of cells for each immunostaining. The cells were washed and suspended in 2 mg/mL of BSA in PBS. We blocked the cells with 2 mg/mL of BSA in PBS for 1 h at room temperature to reduce the non-specific labeling. The primary antibody (Mouse monoclonal antibody specific to human HLA class I antigens) was introduced at a dilution of 1:100 and incubated with the cells for 1 h at room temperature. The cells were then washed three times with 2 mg/mL of BSA in PBS by centrifugation to remove the unconjugated primary antibodies. The primary-antibody-labeled cells were then mixed with the secondary-antibody-SHRIMP conjugates at a concentration of about $10^9$ nanoparticles/mL at room temperature for 1 h. The cells were then washed three times with 2 mg/mL of BSA in PBS. Finally the cells were placed in a petri dish filled with growth media to allow the cell to attach for imaging. The cells were further stained with Calcein AM for fluorescent imaging.

### 2.4. SHG wide-field microscope

We used a SHG wide-field microscope to characterize the SHG properties from $BaTiO_3$ nanocrystals. The excitation was a linearly polarized Ti:sapphire oscillator (150 fs pulse duration centered at 800 nm wavelength with a 76 MHz repetition rate). The laser beam was slightly focused by a lens of 5-cm focal length to reach the peak intensity of 1 GW/cm$^2$ on the sample. The SHG signal was collected by a 100 × 1.4 numerical aperture (NA) oil-immersion objective (UPLSAPO 100XO, Olympus) in the forward direction and imaged directly on an electron multiplying charge coupled device (EMCCD, Andor iXonEM+ 885) with a lens of 20-cm focal length. The excitation was removed by using narrow band-pass filters centered at 400 nm.

### 2.5. Scanning confocal microscope

A standard scanning confocal microscope (Leica, SP5) was used to image the cells labeled by SHRIMPs. The excitation light source consisted of linearly polarized femtosecond laser pulses (Coherent, Chameleon) and the excitation wavelength was centered at 812 nm wavelength. The laser was focused by a 20 × 1.0 NA water-immersion microscope objective. The SHG signal and two-photon fluorescence were collected in epi-geometry simultaneously with two independent channels: SHG channel (400–415 nm) and fluorescent channel (500–550 nm). The transmission signal at the fundamental wavelength is also detected as the third channel.

## 3. Results and discussion

### 3.1. Characterization of $BaTiO_3$ nanocrystals

We started with $BaTiO_3$ nanocrystals in dry powder. X-ray diffraction data (not shown here) confirms that the crystal structure is tetragonal, which is non-centrosymmetric, allowing for efficient SHG without any further treatment. A bright-field transmission electron microscope (TEM) image of $BaTiO_3$ nanocrystals is shown in Fig. 1. The nanocrystals are nearly spherical in shape and between 60 nm and 110 nm in diameter. The $BaTiO_3$ nanocrystals were dispersed in water and treated with ultrasound (Branson digital sonifier 450) to break them into individual nanocrystals.

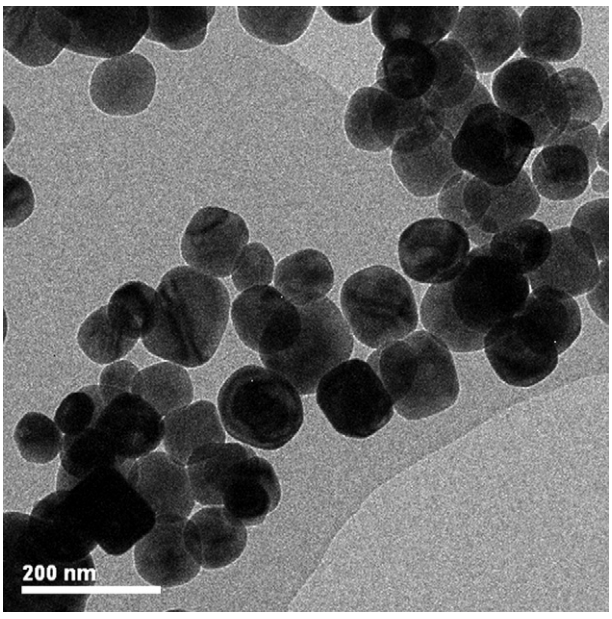


**Fig. 1.** Bright-field TEM image of $BaTiO_3$ nanocrystals.

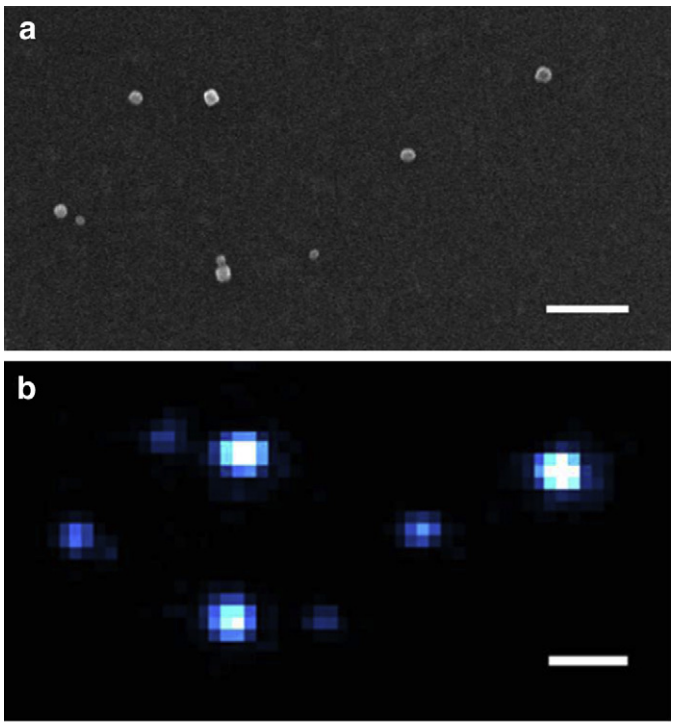


**Fig. 2.** (a) SEM image of $BaTiO_3$ nanocrystals. (b) Wide-field SHG microscopic image of the corresponding $BaTiO_3$ nanocrystals. One-to-one correspondence can be seen between (a) and (b). The scale bars are 500 nm.

Dynamic light scattering measurement (data not shown) indicated that the average size of the nanocrystals was 90 nm in diameter.

### 3.2. SHG from individual $BaTiO_3$ nanocrystals

We prepared isolated individual nanocrystals on an indium-tin-oxide coated glass substrate for SHG characterization. The sample was first imaged by a scanning electron microscope (SEM). Fig. 2(a) is the SEM picture of the $BaTiO_3$ nanocrystals. With the help of the marks on the substrate, we imaged the same area with a SHG wide-field microscope (see Experimental Section 2.4 for details). Fig. 2(b) is the SHG microscopic image of the same nanocrystals as those shown in Fig. 2(a). One-to-one correspondence can be seen between Fig. 2(a) and (b). The spatial resolution in Fig. 2(b) is limited by the diffraction of light at the SHG wavelength. The average SHG photon flux generated from a 90-nm $BaTiO_3$ nanocrystal is on the order of $10^5$ photons/s under the peak excitation intensity of 1 GW/cm$^2$ (150 fs pulse width, 76 MHz repetition rate), which is sufficient for imaging applications. The SHG signal was observed for an hour with less than 5% decrease under continuous excitation. The SHG intensity of individual nanocrystals is different due to the varying sizes and nanocrystal orientations [15].

### 3.3. Surface functionalization and antibody conjugation of $BaTiO_3$ nanocrystals

We functionalized the surface of $BaTiO_3$ nanocrystals with amine groups and further conjugated IgG antibody on the surface to achieve specific labeling. The specific labeling of SHRIMPs was demonstrated through an indirect staining process: the target molecule is first labeled with a primary antibody which is then recognized by a secondary-antibody-SHRIMP conjugate (2nd-Ab-SHRIMP). Scheme 1 shows the processes of functionalization and antibody conjugation of $BaTiO_3$ nanocrystals.

The first step towards functionalizing the SHRIMPs is to attach amine groups on the surface of the $BaTiO_3$ nanocrystal. The amine group attached to the surface of an inorganic material can be used to cross-link to bio-molecules. The bare $BaTiO_3$ nanocrystals were placed in 1 M of nitric acid for 10 min to remove the surface barium ions. It has been reported that the barium ion leaches from the surface of the $BaTiO_3$ nanocrystal into the solution especially in an acid environment [33]. Therefore, after the treatment, we have a "$TiO_2$-like" particle surface. We then placed the treated particles in 10 μM of APTES in ethanol–water–ammonia solution 75/23.5/1.5 v/v/v % at 70 °C for 8 h. The organofunctional silanes act as a bridge between organic and inorganic phases by forming a covalent attachment of organic monolayers [34–36]. As a result, we have accessible amine groups immobilized on the surface of $BaTiO_3$

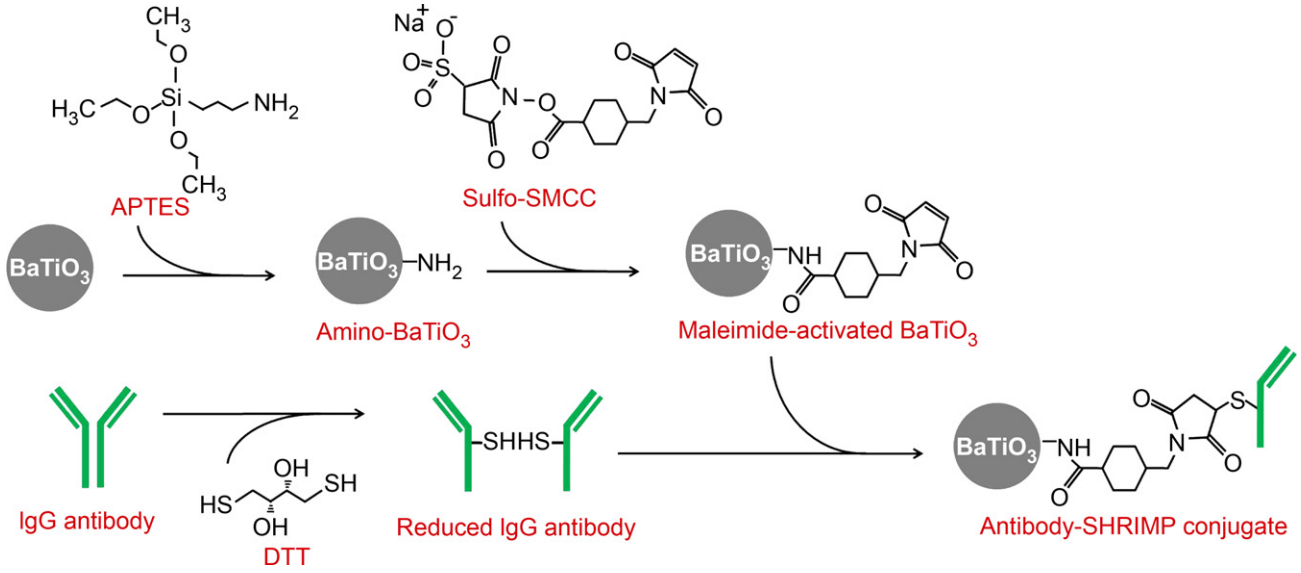


**Scheme 1.** Schematic diagram of the functionalization of primary amine groups and bioconjugation of IgG antibodies on the surface of $BaTiO_3$ nanocrystals. See text for a detailed description.

nanocrystals, referring to as amino-$BaTiO_3$, for further antibody conjugation.

The secondary antibody that we conjugated onto the amino-$BaTiO_3$ is a Donkey anti-Mouse IgG antibody with Cy5 fluorophores on it. The conjugation of the secondary IgG antibodies onto the amino-$BaTiO_3$ is based on the cross-linking reactions between amine and sulfhydryl groups catalyzed by maleimide. These chemical reactions have also been reported for the bioconjugation of QDs [37]. First, we mixed 300 μL of the amino-$BaTiO_3$ solution ($5 \times 10^{11}$ particles/mL in pH 8 NaOH in distilled water) with 200 μL of 22.9 mM sulfo-SMCC at room temperature for 1 h. The amine groups on the SHRIMPs reacted with the sulfo-SMCC to yield maleimide-activated SHRIMPs. Meanwhile, 300 μL of the secondary IgG antibody at 1 mg/mL was mixed with 6 μL of 1 M DTT at room temperature for 30 min. The hinge disulfide bonds on the IgG antibodies were reduced by DTT to yield free sulfhydryl groups. The maleimide-activated SHRIMPs and the reduced antibodies were buffer exchanged by flowing through the desalting columns (NAP-5, GE Healthcare) pre-equilibrated with the exchange buffer (see Experimental Section 2.1 for the solvent composition). The maleimide-activated SHRIMPs and the reduced antibodies were then mixed together at room temperature for 1 h. The 2nd-Ab-SHRIMPs formed when the reduced antibodies covalently coupled to the SHRIMPs through the reaction between the maleimide groups and the free sulfhydryl groups. The conjugation process was then quenched by adding 10 μL of 10 mM 2-mercaptoethanol at room temperature for 30 min. Finally the 2nd-Ab-SHRIMPs were separated from the unconjugated reduced secondary antibodies by using a separation column (Superdex 200, GE Healthcare). The 2nd-Ab-SHRIMPs were stabilized in PBS with 10 mg/ml BSA and 0.1% v/v Tween 20.

### 3.4. Specific labeling of $BaTiO_3$ nanocrystals in an antibody microarray

We verified the effectiveness of specific labeling of the 2nd-Ab-SHRIMPs with a microarray of primary antibodies. Three different types of the primary antibodies and also the buffer solution were printed separately on the microarray (see Experimental Section 2.2 for details). The three types of the primary antibodies were Mouse anti-Human IgG, Goat anti-Human IgG, and Rabbit anti-Human IgG. The Mouse anti-Human IgG was the target primary antibody since the secondary antibody conjugated on the SHRIMPs was an anti-Mouse IgG. Highly specific labeling of the secondary anti-Mouse IgG antibody itself to the target primary antibody was verified with a microarray of the primary antibodies (see Supplementary data for details).

To label the target primary antibodies on the microarray with the 2nd-Ab-SHRIMPs, we first blocked the microarray with PBS with 3% v/v Gelatin and 0.1% v/v Tween 20 for 1 h at room temperature to reduce the non-specific labeling. Then the microarray was incubated with the 2nd-Ab-SHRIMPs at the concentration of $10^{10}$ particles/mL for 2 h at room temperature. Finally the microarray was rinsed with PBS to remove the excess unbound 2nd-Ab-SHRIMPs. The sample was kept wet for imaging with a scanning confocal microscope (Leica, SP5).

Fig. 3 is the microscopic SHG image of the microarray labeled by the 2nd-Ab-SHRIMPs and the corresponding quantitative analysis. The locations of the printed primary antibodies and the buffer solution are shown with dashed circles. Four clear bright spots in a row can be seen in Fig. 3(a), which indicates a high concentration of the 2nd-Ab-SHRIMPs was present at the locations where the target primary antibody was printed. All negative controls show very little SHG signal. From Fig. 3(a), the ratio of the integrated SHG intensity, reflecting the ratio of the number of SHIRMPs, between the target antibody and the negative controls is measured as 1: 0.03: 0.03: 0.05 (Mouse IgG: Goat IgG: Rabbit IgG: Buffer Solution). The standard deviation of the four spots of each sample is shown as the error bar plotted in Fig. 3(b). Therefore, the 2nd-Ab-SHRIMPs showed a highly specific labeling on the primary-antibody microarray.

### 3.5. Specific labeling of $BaTiO_3$ nanocrystals to biological cell membrane proteins in vitro

We further examined the specific labeling of SHRIMPs in a biological cell environment. The human leukocyte antigen (HLA) class I molecule is critical to immune system function in humans because it represents antigenic peptides to T cells. We demonstrated the specific targeting of the HLA class I molecule presented on the HeLa cell surface with $BaTiO_3$ nanocrystals. The HeLa cells were immunostained in suspension with the primary antibody specific to human HLA class I antigens followed by the labeling of 2nd-Ab-SHRIMPs (see Experimental Section 2.3 for details). For comparison, we prepared a control sample where HeLa cells were not stained by the primary antibody under otherwise identical conditions. The cells were prepared in a petri dish and kept alive during the imaging. The cells were imaged with a scanning

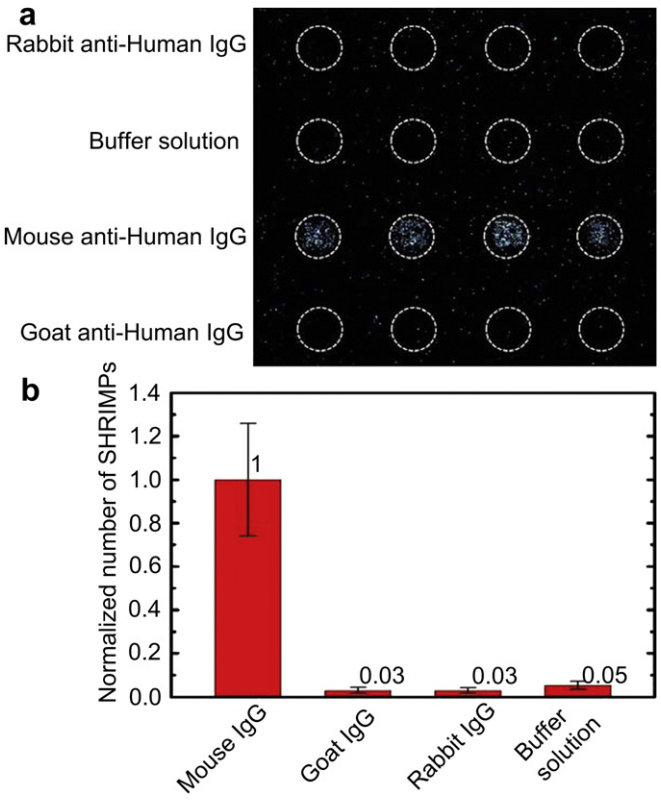


**Fig. 3.** Specific labeling of the 2nd-Ab-SHRIMPs on the primary-antibody microarray. (a) SHG microscopic image of the primary-antibody microarray labeled by the 2nd-Ab-SHRIMPs. The dashed circles show the locations where the target primary antibody (Mouse anti-Human IgG), two other primary antibodies for negative control (Rabbit anti-Human IgG and Goat anti-Human IgG), and the buffer solution were printed. Each of the sample was printed four times in a row in the field of view of this figure. The printing spot size is 90 μm in diameter and the period between the adjacent spots is 200 μm. A high concentration of SHRIMPs can be observed at the locations of the target primary antibodies, showing a highly specific labeling of the 2nd-Ab-SHRIMPs. (b) Quantitative analysis of (a). The ratio of the number of SHRIMPs presenting at the four samples was 1:0.03:0.03:0.05 (Mouse IgG : Goat IgG : Rabbit IgG : Buffer Solution), measured from the integrated SHG intensity. The error bar shows the standard deviation of the four spots of each sample.

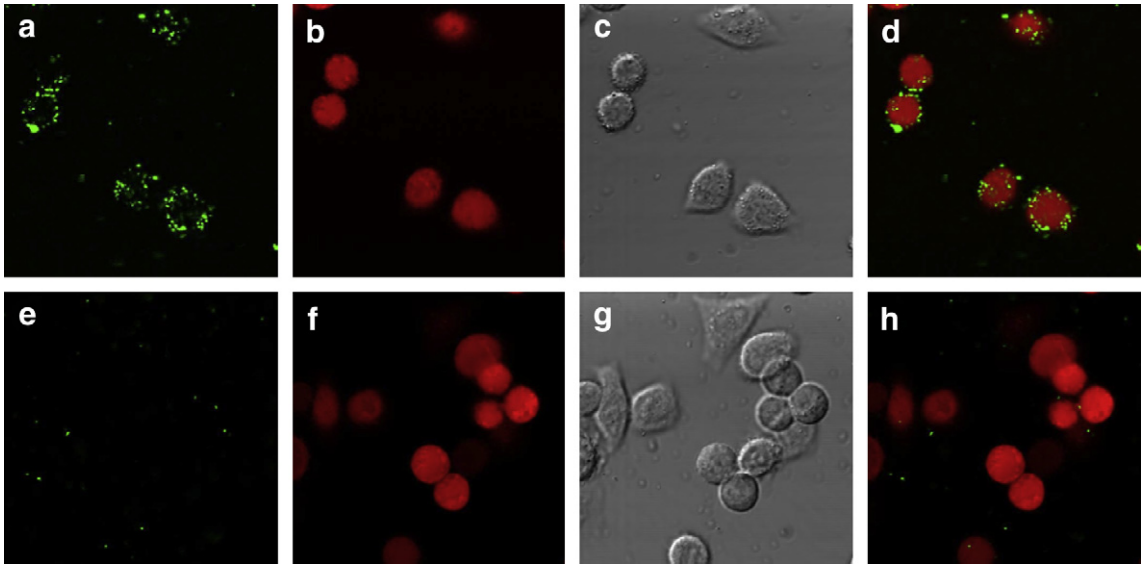


**Fig. 4.** Confocal section images of HeLa cells labeled with the 2nd-Ab-SHRIMPs. (a)-(d) The cells were first labeled with the primary antibody specific to the HLA class I molecules present on the cell membrane and then labeled with the 2nd-Ab-SHRIMPs; (e)–(h) The control sample where the cells were not labeled with primary antibody but under otherwise identical conditions; SHG images are shown in green in (a) and (e); two-photon fluorescence images are shown in red in (b) and (f); transmission images are shown in (c) and (g); and the merged images of SHG images and fluorescence images are shown in (d) and (h). The size of the images is 105 × 105 $\mu m^2$.

confocal microscope (Leica, SP5) under the excitation of femtosecond laser pulses (Coherent, Chameleon) at 812 nm wavelength. Two independent channels, i.e. SHG channel (400–415 nm) and fluorescent channel (500–550 nm) collected the signal in epi-geometry, and a transmission channel collected the fundamental signal in the forward direction. The SHG signal was from the SHRIMPs, and the fluorescent signal was from the Calcein used to stain the cells.

Fig. 4(a)–(d) shows the section images of the cells labeled with 2nd-Ab-SHRIMPs. From these images, we observe a great number of 2nd-Ab-SHRIMPs attached on the cell surface. The SHRIMPs have a great contrast in biological cell environment since the endogenous SHG from the cell components is weak. It is worth noting that SHRIMPs emit SHG signal equally in the forward and backward directions, so the epi-geometry is efficient for signal collection. For comparison, Fig. 4(e)–(h) shows the section images of the HeLa cells in the control sample where almost no 2nd-Ab-SHRIMP is observed on the cell surface. It indicates that the labeling of 2nd-Ab-SHRIMPs on the cell membrane in Fig. 4(a)–(d) is specific to the primary antibody.

## 4. Conclusions

In this work, we report the specific labeling of SHG active $BaTiO_3$ nanocrystals and use them as biomarkers for cell imaging. We demonstrate the surface functionalization of $BaTiO_3$ nanocrystals by immobilizing amine groups on the surface of the nanocrystals. Through the amine groups, we further covalently conjugate IgG secondary antibody onto the nanocrystals. The 2nd-Ab-SHRIMPs are able to label the specific primary antibody and therefore can be applied to label molecules of interest through indirect staining. Highly specific labeling of the SHRIMPs (less than 5% non-specific labeling) was observed on the primary-antibody microarray. Moreover, we demonstrate that SHRIMPs are efficient biomarkers for in vitro cell imaging by targeting the SHRIMPs to specific biological cell membrane proteins. The development of surface functionalization and bioconjugation of SHRIMPs provides the opportunities of applying SHRIMPs to biological studies.

## Acknowledgements

The authors thank Keith Harshman, Johann Weber, Floriane Consales, and John Wang in University of Lausanne for the help of microarray preparation. The authors thank Marie-Agnes Doucey, Sylvian Bron, and Pei-Jiun Chen in University of Lausanne for the discussion of the antibodies and nanocrystals staining. The authors thank Paul Bowen for providing the nanocrystals, Marc Chambon and Nathalie Ballanfat for the help of HeLa cell preparation. The authors also thank Stephen Quake, Stavros Stavrakis, and Jerrod Schwartz for helpful discussions on the colloidal stabilization. This project is supported by National Center of Competence in Research (NCCR), Quantum Photonics.

## Appendix. Supplementary data

The supplementary data associated with this article can be found in the on-line version at doi:10.1016/j.biomaterials.2009.11.096.

## Appendix

Figures with essential colour discrimination. Figs. 2–4 in this article may be difficult to interpret in black and white. The full colour images can be found in the on-line version, at doi:10.1016/j.biomaterials.2009.11.096.

## References

[1] Chalfie M, Tu Y, Euskirchen G, Ward WW, Prasher DC. Green fluorescent protein as a marker for gene-expression. Science 1994;263(5148):802–5.
[2] Giepmans BNG, Adams SR, Ellisman MH, Tsien RY. Review – the fluorescent toolbox for assessing protein location and function. Science 2006;312(5771):217–24.
[3] Xu C, Zipfel W, Shear JB, Williams RM, Webb WW. Multiphoton fluorescence excitation: new spectral windows for biological nonlinear microscopy. Proc Natl Acad Sci U S A 1996;93(20):10763–8.
[4] Chan WCW, Nie SM. Quantum dot bioconjugates for ultrasensitive nonisotopic detection. Science 1998;281(5385):2016–8.
[5] So PTC, Dong CY, Masters BR, Berland KM. Two-photon excitation fluorescence microscopy. Annu Rev Biomed Eng 2000;2:399–429.

[6] Campagnola PJ, Loew LM. Second-harmonic imaging microscopy for visualizing biomolecular arrays in cells, tissues and organisms. Nat Biotechnol 2003;21(11):1356–60.
[7] Chu SW, Chen SY, Tsai TH, Liu TM, Lin CY, Tsai HJ, et al. In vivo developmental biology study using noninvasive multi-harmonic generation microscopy. Opt Express 2003;11(23):3093–9.
[8] Zipfel WR, Williams RM, Christie R, Nikitin AY, Hyman BT, Webb WW. Live tissue intrinsic emission microscopy using multiphoton-excited native fluorescence and second harmonic generation. Proc Natl Acad Sci U S A 2003;100(12):7075–80.
[9] Brown E, McKee T, diTomaso E, Pluen A, Seed B, Boucher Y, et al. Dynamic imaging of collagen and its modulation in tumors in vivo using second-harmonic generation. Nat Med 2003;9(6):796–800.
[10] Konig K, Riemann I. High-resolution multiphoton tomography of human skin with subcellular spatial resolution and picosecond time resolution. J Biomed Opt 2003;8(3):432–9.
[11] Jung Y, Tong L, Tanaudommongkon A, Cheng JX, Yang C. In vitro and in vivo nonlinear optical imaging of silicon nanowires. Nano Lett 2009;9(6):2440–4.
[12] Tai SP, Wu Y, Shieh DB, Chen LJ, Lin KJ, Yu CH, et al. Molecular imaging of cancer cells using plasmon-resonant-enhanced third-harmonic-generation in silver nanoparticles. Adv Mater 2007;19(24):4520.
[13] Yelin D, Silberberg Y. Laser scanning third-harmonic-generation microscopy in biology. Opt Express 1999;5(8):169–75.
[14] Pu Y, Centurion M, Psaltis D. Harmonic holography: a new holographic principle. Appl Opt 2008;47(4):A103–10.
[15] Hsieh CL, Grange R, Pu Y, Psaltis D. Three-dimensional harmonic holographic microcopy using nanoparticles as probes for cell imaging. Opt Express 2009;17(4):2880–91.
[16] Johnson JC, Yan HQ, Schaller RD, Petersen PB, Yang PD, Saykally RJ. Near-field imaging of nonlinear optical mixing in single zinc oxide nanowires. Nano Lett 2002;2(4):279–83.
[17] Brasselet S, Le Floc'h V, Treussart F, Roch JF, Zyss J, Botzung-Appert E, et al. In situ diagnostics of the crystalline nature of single organic nanocrystals by nonlinear microscopy. Phys Rev Lett 2004;92(20):4.
[18] Xuan LL, Brasselet S, Treussart F, Roch JF, Marquier F, Chauvat D, et al. Balanced homodyne detection of second-harmonic generation from isolated subwavelength emitters. Appl Phys Lett 2006;89(12):121118.
[19] Delahaye E, Tancrez N, Yi T, Ledoux I, Zyss J, Brasselet S, et al. Second harmonic generation from individual hybrid MnPS3-based nanoparticles investigated by nonlinear microscopy. Chem Phys Lett 2006;429(4–6):533–7.
[20] Bonacina L, Mugnier Y, Courvoisier F, Le Dantec R, Extermann J, Lambert Y, et al. Polar Fe(IO3)(3) nanocrystals as local probes for nonlinear microscopy. Appl Phys B 2007;87(3):399–403.
[21] Nakayama Y, Pauzauskie PJ, Radenovic A, Onorato RM, Saykally RJ, Liphardt J, et al. Tunable nanowire nonlinear optical probe. Nature 2007;447(7148). 1098–U1098.
[22] Sandeau N, Le Xuan L, Chauvat D, Zhou C, Roch JF, Brasselet S. Defocused imaging of second harmonic generation from a single nanocrystal. Opt Express 2007;15(24):16051–60.
[23] Kachynski AV, Kuzmin AN, Nyk M, Roy I, Prasad PN. Zinc oxide nanocrystals for nonresonant nonlinear optical microscopy in biology and medicine. J Phys Chem C 2008;112(29):10721–4.
[24] Le Xuan L, Zhou C, Slablab A, Chauvat D, Tard C, Perruchas S, et al. Photostable second-harmonic generation from a single KTiOPO4 nanocrystal for nonlinear microscopy. Small 2008;4(9):1332–6.
[25] Rodriguez EV, de Araujo CB, Brito-Silva AM, Ivanenko VI, Lipovskii AA. Hyper-Rayleigh scattering from BaTiO3 and PbTiO3 nanocrystals. Chem Phys Lett 2009;467(4–6):335–8.
[26] Kuo TR, Wu CL, Hsu CT, Lo W, Chiang SJ, Lin SJ, et al. Chemical enhancer induced changes in the mechanisms of transdermal delivery of zinc oxide nanoparticles. Biomaterials 2009;30(16):3002–8.
[27] Wnuk P, Le Xuan L, Slablab A, Tard C, Perruchas S, Gacoin T, et al. Coherent nonlinear emission from a single KTP nanoparticle with broadband femtosecond pulses. Opt Express 2009;17(6):4652–8.
[28] Rodriguez EM, Speghini A, Piccinelli F, Nodari L, Bettinelli M, Jaque D, et al. Multicolour second harmonic generation by strontium barium niobate nanoparticles. J Phys D Appl Phys 2009;42(10):4.
[29] Delahaye E, Sandeau N, Tao Y, Brasselet S, Clement R. Synthesis and second harmonic generation microscopy of nonlinear optical efficient hybrid nanoparticles embedded in polymer films. Evidence for intra- and inter-nanoparticles orientational synergy. J Phys Chem C 2009;113(21):9092–100.
[30] Extermann J, Bonacina L, Cuna E, Kasparian C, Mugnier Y, Feurer T, et al. Nanodoublers as deep imaging markers for multi-photon microscopy. Opt Express 2009;17(17):15342–9.
[31] Dadap JI, Shan J, Eisenthal KB, Heinz TF. Second-harmonic Rayleigh scattering from a sphere of centrosymmetric material. Phys Rev Lett 1999;83(20):4045–8.
[32] Campagnola PJ, Wei MD, Lewis A, Loew LM. High-resolution nonlinear optical imaging of live cells by second harmonic generation. Biophys J 1999;77(6):3341–9.
[33] Yoon DH, Lee BI, Badheka P, Wang XY. Barium ion leaching from barium titanate powder in water. J Mater Sci Mater Electron 2003;14(3):165–9.
[34] Helmy R, Fadeev AY. Self-assembled monolayers supported on $TiO_2$: comparison of C18H37SiX3 (X = H, Cl, OCH3C18H37Si(CH3)2C1, and C18H37PO(OH)(2). Langmuir 2002;18(23):8924–8.
[35] Moses PR, Wier LM, Lennox JC, Finklea HO, Lenhard JR, Murray RW. Chemically modified electrodes. 9. X-ray photoelectron-spectroscopy of alkylamine-silanes bound to metal-oxide electrodes. Anal Chem 1978;50(4):576–85.
[36] Mornet S, Elissalde C, Hornebecq V, Bidault O, Duguet E, Brisson A, et al. Controlled growth of silica shell on Ba0.6Sr0.4TiO3 nanoparticles used as precursors of ferroelectric composites. Chem Mater 2005;17(17):4530–6.
[37] Xing Y, Chaudry Q, Shen C, Kong KY, Zhau HE, Wchung L, et al. Bioconjugated quantum dots for multiplexed and quantitative immunohistochemistry. Nat Protoc 2007;2(5):1152–65.